JOURNAL OF GEOPHYSICAL RESEARCH, VOL. 114, B01311, doi:10.1029/2008JB005749, 2009

Scaling of small repeating earthquakes explained by interaction of seismic and aseismic slip in a rate and state fault model

Ting Chen[1] and Nadia Lapusta[2]

Received 15 April 2008; revised 24 October 2008; accepted 6 November 2008; published 24 January 2009.

[1] Because of short recurrence times and known locations, small repeating earthquakes present a rare predictable opportunity for detailed field observations. They are used to study fault creeping velocities, earthquake nucleation, stress drops, and other aspects of tectonophysics, earthquake mechanics, and seismology. An intriguing observation about repeating earthquakes is their scaling of recurrence time with seismic moment, which is significantly different from the scaling based on a simple conceptual model of circular ruptures with stress drop independent of seismic moment and no aseismic slip. Here we show that a model of repeating earthquakes based on laboratory-derived rate and state friction laws reproduces the observed scaling. In the model, a small fault patch governed by steady state velocity-weakening friction is surrounded by a much larger velocity-strengthening region. Long-term slip behavior of the fault is simulated using a methodology that fully accounts for both aseismic slip and inertial effects of occasional seismic events. The model results in repeating earthquakes with typical stress drops and sizes comparable with observations. For a fixed set of friction parameters, the observed scaling is reproduced by varying the size of the velocity-weakening patch. In simulations, a significant part of slip on the velocity-weakening patches is accumulated aseismically, even though the patches also produce seismic events. The proposed model supplies a laboratory-based framework for interpreting the wealth of observations about repeating earthquakes, provides indirect evidence that rate and state friction acts on natural faults, and has important implications for possible scenarios of slip partition into seismic and aseismic parts.

Citation: Chen, T., and N. Lapusta (2009), Scaling of small repeating earthquakes explained by interaction of seismic and aseismic slip in a rate and state fault model, *J. Geophys. Res.*, *114*, B01311, doi:10.1029/2008JB005749.

1. Introduction

[2] Repeating earthquakes are seismic events that repeatedly occur in the same location with similar seismic signal. Sequences of small repeating earthquakes have been found on a number of faults [*Ellsworth and Dietz*, 1990; *Vidale et al.*, 1994; *Nadeau and Johnson*, 1998; *Bürgmann et al.*, 2000; *Igarashi et al.*, 2003; *Peng and Ben-Zion*, 2005; *Chen et al.*, 2007]. Since their recurrence times range from a fraction of a year to several years and their locations are known, small repeating earthquakes are an excellent observation target. This has been exploited in a number of studies, such as the San Andreas Fault Observatory at Depth (SAFOD) drilling project [*Hickman et al.*, 2004] (Figure 1). Repeating earthquakes are used to study an increasingly richer array of problems, from fault creeping velocities and postseismic slip to earthquake interaction and stress drops [*Ellsworth and Dietz*, 1990; *Vidale et al.*, 1994; *Marone et al.*, 1995; *Nadeau and Johnson*, 1998; *Schaff et al.*, 1998; *Nadeau and McEvilly*, 1999; *Bürgmann et al.*, 2000; *Igarashi et al.*, 2003; *Nadeau et al.*, 2004; *Schaff and Beroza*, 2004; *Matsubara et al.*, 2005; *Peng and Ben-Zion*, 2005; *Allmann and Shearer*, 2007; *Chen et al.*, 2007; *Dreger et al.*, 2007]. To assimilate and properly interpret the wealth of data on small repeating earthquakes, it is important to construct a realistic model of their occurrence.

[3] One of the intriguing observations about small repeating earthquakes is the scaling of their seismic moment M_0 with the recurrence time T as

$$T \propto M_0^{0.17}. \tag{1}$$

This scaling has been first pointed out by *Nadeau and Johnson* [1998] for repeating earthquakes along the Parkfield segment of the San Andreas fault, and it has since been confirmed in other tectonic environments [*Chen et al.*, 2007]. However, a simple conceptual model of these events as circular ruptures, with stress drop $\Delta\tau$ independent of the seismic moment M_0 and slip equal to $V_L T$, where V_L

[1]Seismological Laboratory, California Institute of Technology, Pasadena, California, USA.
[2]Division of Engineering and Applied Science and Seismological Laboratory, California Institute of Technology, Pasadena, California, USA.

0148-0227/09/2008JB005749$09.00

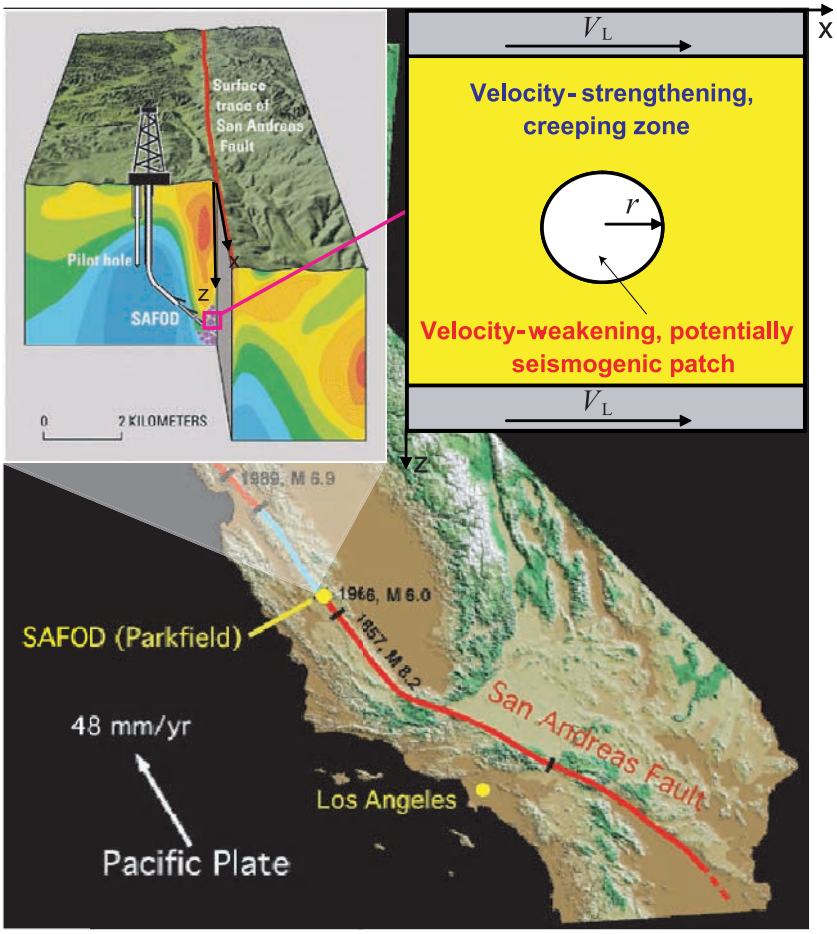

Figure 1. Schematics of the model. To simulate repeating earthquakes, such as the targets of SAFOD drilling project on the Parkfield segment (shown in blue) of the San Andreas fault, we consider a segment of a vertical strike-slip fault embedded into an elastic medium and governed by rate and state friction laws. On the fault, a small, potentially seismogenic, patch with steady state velocity-weakening properties (shown in white) is surrounded by a creeping, velocity-strengthening segment (shown in yellow). Outside of the simulated fault segment, steady sliding is imposed with the long-term slip velocity V_L. The creeping (yellow) zone is chosen to be large enough so that the model behavior does not depend on its size.

is the long-term slip velocity (also called slip rate) accommodated by the fault segment, results in [*Nadeau and Johnson*, 1998; *Beeler et al.* 2001]

$$T = \Delta\tau^{2/3} M_0^{1/3} / (1.81 \mu V_L) \propto M_0^{1/3}, \qquad (2)$$

where μ is the shear modulus of the bulk. Note that this model assumes that all slip at the location of repeating earthquakes is accumulated seismically. The observed and theoretical scalings have different exponents as well as different absolute values of recurrence times. If T is measured in seconds and M_0 is measured in dyne centimeters [*Nadeau and Johnson*, 1998; *Chen et al.*, 2007], the Parkfield observations are well approximated by $T = 7 \times 10^4 M_0^{0.17}$, while the theoretical model gives $T \approx 2.4\ M_0^{1/3}$ for typical values $\Delta\tau = 3$ MPa, $\mu = 30$ GPa, and $V_L = 23$ mm/a. Thus the observed recurrence times are much larger than the theoretical ones for moment magnitudes typical for small repeating earthquakes. Several explanations for the discrepancy in scaling and recurrence times have been proposed [*Nadeau and Johnson*, 1998; *Beeler et al.*, 2001; *Anooshehpoor and Brune*, 2001; *Sammis and Rice*, 2001]. In the work of *Nadeau and Johnson* [1998], it was interpreted as an indication of the dependence of stress drop on seismic moment, with higher stress drops for smaller events. However, to fit the observed recurrence times, stress drops for the smallest repeating earthquakes would have to be as high as 2500 MPa [*Nadeau and Johnson*, 1998]. Not only the physical basis for stress drops of such high values is unclear [*Beeler et al.*, 2001], but also recent seismic estimates of stress drops for repeating earthquakes in Parkfield [*Imanishi et al.*, 2004; *Allmann and Shearer*, 2007] have pointed to values of the order of 1 to 10 MPa, the typical range for earthquakes in general [*Abercrombie*, 1995]. The work of *Sammis and Rice* [2001] presented a model with the observed scaling $T \propto M_0^{1/6}$ in which repeating earthquakes occur on small seismogenic patches located at the boundary between

much larger creeping and locked regions. The small patches are assumed to be much weaker than the larger locked region, so that the patches fail many times before the larger region is ready to rupture. The model achieves the correct scaling because of stress concentration at the boundary. The corresponding stress drops are relatively small, 0.5 MPa to 0.08 MPa for the larger locked regions with radii of 100 m to 2 km. Such small stress drops would correspond to much smaller slips than would be necessary to accommodate the long-term slip of the fault segment, and it is postulated that most of the slip at the location of repeating earthquakes would be accumulated when the larger locked region fails. Hence the model of *Sammis and Rice* [2001] predicts that there are larger locked regions within the creeping section of the San Andreas fault that should fail in much larger earthquakes than the repeating events discussed here. However, currently there is no evidence for such events. The potential importance of aseismic slip at the location of repeating earthquakes was highlighted in the study by *Beeler et al.* [2001] which used a spring-slider (one-degree-of-freedom) model governed by a constitutive law that incorporated strain hardening in the interseismic period. In the model, part of the accumulated slip was aseismic, because of strain-hardening behavior, and the resulting scaling of the seismic moment with the recurrence time had a trend similar to the one observed. However, *Beeler et al.* [2001] pointed out that there was no experimental evidence for the strain-hardening law used in the model.

[4] In this work, we demonstrate that the observed scaling is reproduced in a model of repeating earthquakes that treats them as frictional instabilities on a fault in an elastic medium and incorporates laboratory-derived rate and state friction laws [*Dieterich*, 1979, 1981; *Ruina*, 1983; *Marone*, 1998; *Dieterich*, 2007, and references therein]. Rate and state friction laws have been successfully used to model a number of fault slip phenomena as discussed in a recent review by *Dieterich* [2007]. For the case of constant normal stress σ, a commonly adopted form of the law is

$$\tau = \sigma[f_0 + a\ln(V/V_0) + b\ln(V_0\theta/L)] \tag{3}$$

$$d\theta/dt = 1 - V\theta/L, \tag{4}$$

where V is slip velocity, θ is a state variable, L is the characteristic slip for state variable evolution, V_0 and f_0 are the reference slip velocity and friction coefficient respectively, and a and b are rate and state parameters. We use a regularized version of the law at $V = 0$ [*Lapusta et al.*, 2000]. The "aging" formulation (4) for the state variable evolution incorporates strengthening (or healing) of the fault in stationary contact, a feature needed to explain laboratory observations [*Beeler et al.*, 1994]. Recent experiments [*Bayart et al.*, 2006] suggested that the "slip" formulation [*Dieterich*, 1979, 1981; *Ruina*, 1983] may be a better description of the friction response for the range of slip velocities studied in the experiments. Perhaps a combined law, of the type proposed by *Kato and Tullis* [2001], would be the most appropriate one to use. Different state evolution laws cause differences in the process of earthquake nucleation [*Ampuero and Rubin*, 2008] and hence it would be important to examine the behavior of our model with other state evolution laws. We discuss this issue further in section 6.

[5] The parameter combination $a - b > 0$ corresponds to steady state velocity-strengthening properties while $b - a > 0$ corresponds to steady state velocity weakening. In the following, we refer to fault regions as being velocity strengthening or velocity weakening with the implicit understanding that the characterization applies to the steady state behavior. Velocity-strengthening fault zones tend to respond to slow loading with stable, aseismic slip, while velocity-weakening zones of sufficiently large sizes can produce inertially controlled seismic events [*Rice and Ruina*, 1983; *Dieterich*, 1992; *Rubin and Ampuero*, 2005]. Sufficiently small regions on velocity-weakening faults can also slip aseismically, leading to aseismic nucleation processes. For $0.5 < a/b < 1$, the range of parameters that includes the representative laboratory values of a and b used in this work, the half size of the slipping region capable of producing seismic slip under slow loading can be estimated as [*Rubin and Ampuero*, 2005]

$$h^*_{RA} = \hat{\mu}bL/\left(\pi\sigma(b-a)^2\right), \tag{5}$$

with $\hat{\mu} = \mu$ for antiplane sliding and $\hat{\mu} = \mu/(1 - \nu)$ for inplane sliding, where ν is the Poisson's ratio. The 3-D nucleation estimates obtained from the same considerations as the 2-D estimates of *Rubin and Ampuero* [2005] would be larger by a factor of $\pi^2/4$ (A. Rubin, private communication, 2008).

2. Model for Repeating Earthquakes

[6] We consider a planar fault embedded in an elastic medium and numerically simulate the behavior of a finite fault region around the location of a repeating earthquake (Figure 1). The elastodynamic properties of the medium are as follows: shear modulus $\mu = 30$ GPa, Poisson's ratio $\nu = 0.25$, the shear wave speed $c_s = 3$ km/s, and the P wave speed $c_p = 5.2$ km/s. On the fault, a potentially seismogenic, circular patch of radius r is surrounded by a much larger creeping zone. The difference in behavior between the patch and the surrounding area is achieved by assigning velocity-weakening properties, $b - a > 0$, to the patch and velocity-strengthening properties, $a - b > 0$, to the surrounding fault zone. In all simulations, the size of the velocity-strengthening zone is kept at least four times larger than the patch radius. Outside the velocity-strengthening zone, steady sliding with the long-term slip velocity V_L is imposed, to model steady creep (i.e., slow slip) of the surrounding fault area. We solve for spontaneous slip history in this model using the 3-D simulation methodology of N. Lapusta and Y. Liu (3D boundary-integral modeling of spontaneous earthquake sequences and aseismic slip, submitted to *Journal of Geophysical Research*, 2008), which fully resolves all aspects of seismic and aseismic behavior of the fault, including long aseismic periods of slip with velocities of the order of millimeters per year, accelerating and decelerating aseismic slip in the interseismic period, all inertial effects during simulated earthquakes with slip velocities of the order of meters per second, and postseismic slip. The model of repeating earthquakes as

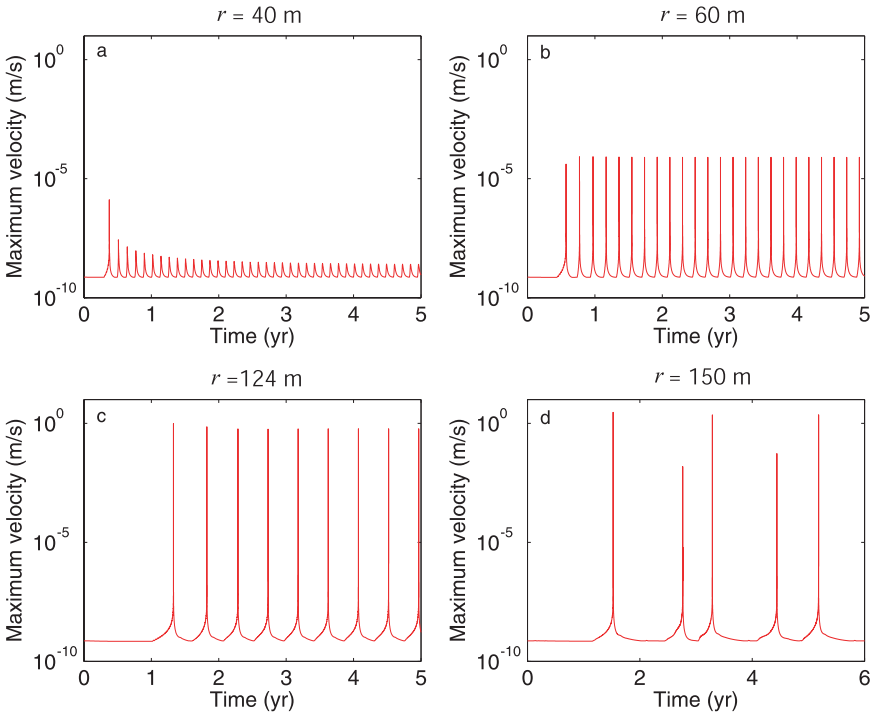

Figure 2. Maximum slip velocity over the fault as a function of simulated time, plotted for different radii of the velocity-weakening patch: (a) $r = 40$, (b) $r = 60$, (c) $r = 124$, and (d) $r = 150$ m. Smaller values of r result in aseismic behavior of the patch, with slip velocities never approaching seismic values (Figures 2a and 2b), while larger values of r result in sequences of repeating earthquakes (Figures 2c and 2d). This behavior is consistent with stability properties of rate and state faults.

shear ruptures on seismogenic patches embedded into a larger creeping fault region has been shown to be consistent with the observed postseismic response of repeating aftershocks on the San Andreas fault [*Schaff et al.*, 1998]. *Kato* [2004] used a similar (but quasi-dynamic) model to study interactions between two sequences of repeating earthquakes.

[7] In all our simulations, we use effective normal stress $\sigma = 50$ MPa and the reference friction coefficient $f_0 = 0.6$ at $V_0 = 1$ μm/s. In simulations presented in section 3 and part of section 4, we adopt the following values of rate and state parameters representative of laboratory results: $L = 160$ μm, $a = 0.015$, and $b - a = 0.004$ for the velocity-weakening patch, and $a = 0.019$ and $a - b = 0.004$ for the surrounding velocity-strengthening zone. To investigate how the behavior varies with friction parameters, we have explored a range of values for the rate and state parameters a and b (section 4), making the velocity-weakening parameter $(b - a)$ on the patch two times larger and two times smaller and studying a different value of a. In each case, the properties of the velocity-strengthening zone are assigned by switching the values of a and b. Two values of long-term slip rate are used: $V_L = 23$ mm/a (based on the work by *Nadeau and Johnson* [1998]) and $V_L = 4.5$ mm/a. The fault is discretized into rectangular cells which are ~10–20 times smaller than $h^*_{RR} = \hat{\mu}\,\pi L/[4\,\sigma\,(b - a)]$ [*Rice and Ruina*, 1983]. Such discretization is adequate for both nucleation processes and the cohesive zone at the rupture tip as discussed by *Day et al.* [2005] and Lapusta and Liu (submitted manuscript, 2008). The quasi-static value of the cohesive zone is related to h^*_{RR} through the factor of $(b - a)/b$. The results of several conceptually important simulations were confirmed with finer resolutions.

3. Model Response for Different Patch Sizes

[8] As predicted by studies of stability of frictional sliding (section 1), much of the velocity-strengthening part of the fault accumulates slip through stable sliding with the imposed long-term slip rate V_L. The behavior of the velocity-weakening patch depends on its radius, consistent with the findings of stability studies that a sufficiently large velocity-weakening region is required for unstable slip. For sufficiently small values of r, the velocity-weakening patch accumulates slip through perturbed but aseismic sliding, with slip velocities that never deviate too much from the long-term slip velocity V_L. Velocity-weakening patches of larger sizes produce repeating earthquakes. This is illustrated in Figure 2 which shows the history of maximum slip velocity on the fault for four values of the patch radius r. For all values of r and for most of the simulated time, the maximum slip velocity is close to the imposed long-term velocity of $V_L = 23$ mm/a (which translates into a value slightly smaller than 10^{-9} m/s), because of stable sliding of the velocity-strengthening zone away from the velocity-weakening patch. The presence of the patch results in periodic increases of maximum slip velocity. We take 1 cm/s as the value separating seismic and aseismic slip rates. For the properties used in this section ($L = 160$ μm, $a = 0.015$, $b - a = 0.004$, $\sigma = 50$ MPa), the radius of the smallest patch that results in seismic slip in our simulations is $r = 83$ m. Values of r smaller than 83 m result in aseismic

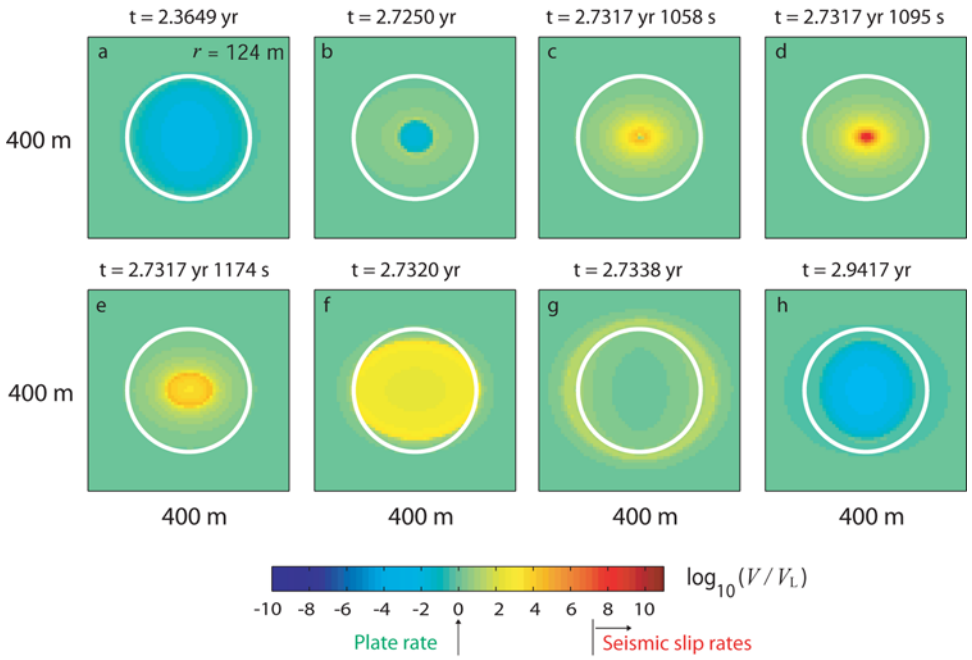

Figure 3. Snapshots of slip velocity distribution for one earthquake cycle and $r = 124$ m. Slip velocity is color coded on the logarithmic scale. The seismic range of slip velocities is indicated by red, and slip velocities close to the long-term slip velocity are indicated by green. The location of the patch is outlined by a white circle. The simulated fault region is 800 m $\times$ 800 m; only a part of it is shown in each snapshot. Much of the slip on the patch is accumulated aseismically (orange, yellow, and green). Note that in this simulation, the extent of seismic slip is smaller than the size of the patch. The simulations fully account for both slow aseismic slip and inertial effects during seismic events.

slip velocity at all times, although the maximum slip velocity during accelerations of the patch increases as r approaches the critical size (Figures 2a and 2b). Values of r larger than 83 m result in periodic excursions of slip velocity to values larger than 1 cm/s, indicating repeating earthquakes (Figures 2c and 2d). The seismogenic patches can create additional complexity in slip patterns. For example, $r = 150$ m results in transient increases of slip velocity before repeating earthquakes (Figure 2d), as discussed further in section 3.2. The estimate (5) gives $h^*_{RA} = 36$ m for antiplane sliding and $h^*_{RA} = 48$ m for inplane sliding, which is consistent, in view of the 3-D factor $\pi^2/4$, with the critical patch radius $r = 83$ m of our simulations. Note that the model with $r = 94$ m has the maximum slip velocity of 0.07 m/s while the model with $r = 100$ m has the maximum slip velocity of 0.17 m/s. Hence changing the threshold separating aseismic and seismic slip velocities to 0.1 m/s would result in the critical patch size between 94 m and 100 m.

3.1. Response of Patches That Are Just Large Enough to Produce Seismic Events

[9] One seismic cycle from a simulation with $r = 124$ m is illustrated in Figure 3. This patch size is only slightly larger than the critical patch size of 83 m. At some point in time during the interseismic period, most of the velocity-weakening patch is locked; Figure 3a shows the distribution of slip velocity over a part of the fault close to the velocity-weakening patch at the time of 0.08 years after a seismic event (which occurs at the simulated time of 2.28 years). As the simulated time progresses, the locked area shrinks because of penetration of stable slip from the velocity-strengthening zone surrounding the patch (Figure 3b). This is consistent with the stability properties of velocity-weakening regions in which slip over small zones can be stable. Eventually, slip accelerates (Figure 3c) and fast (seismic) slip occurs (Figure 3d) at the simulated time of 2.73 years. The interseismic period in this case is 0.45 years. Postseismic slip continues on the patch for a while (Figures 3e and 3f), eventually affecting the velocity-strengthening zone surrounding the patch (Figure 3g). Finally, the patch becomes locked again (Figure 3h), and the earthquake cycle repeats. It is important to point out that, for this value of r, the extent of seismic slip, shown in red in Figure 3, is a small fraction of the velocity-weakening patch. This means that sizes of repeating earthquakes inferred on the basis of seismic data may be smaller than the underlying velocity-weakening patches that cause them.

[10] In this model, a significant part of slip at the location of the velocity-weakening patch is accumulated aseismically. Continuing with the example of $r = 124$ m, let us consider the history of maximum slip velocity and moment accumulation on the patch (Figure 4). On the scale of years, the history of maximum slip velocity on the fault (Figure 4a) points to the occurrence of repeating earthquakes, as already discussed. The cumulative moment release on the velocity-weakening patch (Figure 4d) has the corresponding step-like nature, with most moment released near the time of the seismic events. However, even on this scale of years, we already see that a significant fraction of moment, about one

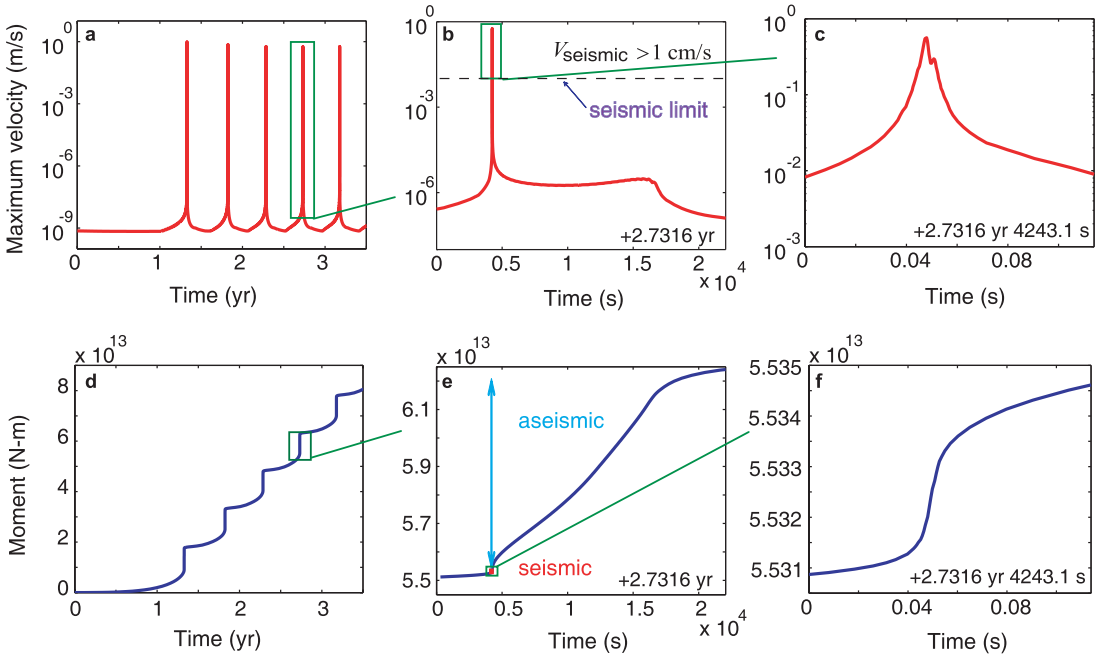

Figure 4. (a–c) Maximum slip velocity over the fault as a function of simulated time, plotted on different temporal scales, for r = 124 m. (d–f) Cumulative moment release on the velocity-weakening patch for the same time intervals. We see that seismic moment, defined as the moment released with the maximum slip velocity larger than 1 cm/s, is only a small fraction of the total moment released on the patch and that there is significant preseismic and postseismic slip.

third, is released during aseismic periods, when the maximum slip velocity is within an order of magnitude from the long-term slip velocity V_L = 23 mm/a. This is due to penetration of slip from the creeping region into the locked patch, as shown in Figure 3b. On the scale of tens of thousands of seconds or several hours (Figures 4b and 4e), the seismic event is still too short to see in detail, but it is clear, from comparison of panels 4b and 4e, that the moment released with seismic slip velocities is much smaller than the moment released during postseismic slip with slip velocities of the order of 10^{-6} m/s. The histories of the maximum slip velocity and moment released during the seismic event itself are shown in Figures 4c and 4f. The moment magnitude of the seismic event is M_w = 0.9. In this simulation, the ratio of seismic and total moments on the patch is less than 0.01, indicating that more than 99% of slip on the patch is accumulated aseismically. Note that we find such a small contribution of seismic moment only for patch sizes that are just large enough to produce seismic slip. That makes intuitive sense, since slightly smaller patches would be completely aseismic.

3.2. Response of Larger Patches

[11] As shown in section 3.1, the velocity-weakening patches that are just large enough to be seismogenic produce seismic slip only over a part of the patch and result in very small ratios of seismic to total slip on the patch, less than 0.01. For larger patches, seismic slip extends to the entire area of the patch. The change in the behavior occurs rather sharply at about r = 130 m. As an illustration, consider one seismic cycle from a simulation with r = 150 m shown in Figure 5. At some point in time during the interseismic period, most of the velocity-weakening patch is locked (Figure 5a), similarly to the case of r = 124 m. Figure 5a corresponds to the time of 0.07 years after a seismic event (which occurs at the simulated time of 5.18 years). As the simulated time progresses, the locked area shrinks because of penetration of stable slip from the velocity-strengthening zone surrounding the patch, until the entire patch slides aseismically (Figure 5b). The middle of the patch experiences accelerated slip, with slip velocity that briefly reaches the seismic slip threshold of 0.01 m/s at a small portion of the patch (Figure 5c), before slip velocities decrease (Figure 5d) and most of the patch becomes locked again (Figure 5e). The creep-in of the slow slip repeats, causing another acceleration of slip in the middle of the patch (Figures 5f–5h) which finally results in a patch-spanning seismic event (Figures 5i and 5j) at the time of 6.81 years. The interseismic period in this case is 1.63 years. The event is followed by postseismic slip (Figure 5k). In this case, the moment magnitude of seismic events is M_w = 2.9 and the ratio of seismic to total moment on the patch is about 0.3.

[12] Hence we find that, for r = 150 m, the entire patch is involved in seismic slip eventually. In that regard, the behavior is similar to that of even larger patches, as discussed in the following. However, there are also similarities with the case of r = 124 m. First, the entire patch experiences aseismic slip before a dynamic event. Second, the behavior of slip is still nearly axisymmetric, modulated only by the difference between the antiplane (Mode III) and inplane (Mode II) sliding directions. In part, seismic slip still originates in the middle of the patch and expands toward the boundaries.

[13] For larger patches, the middle part of the patch remains locked when a dynamic event starts. Figure 6 shows one seismic cycle from a simulation with r = 350 m. As

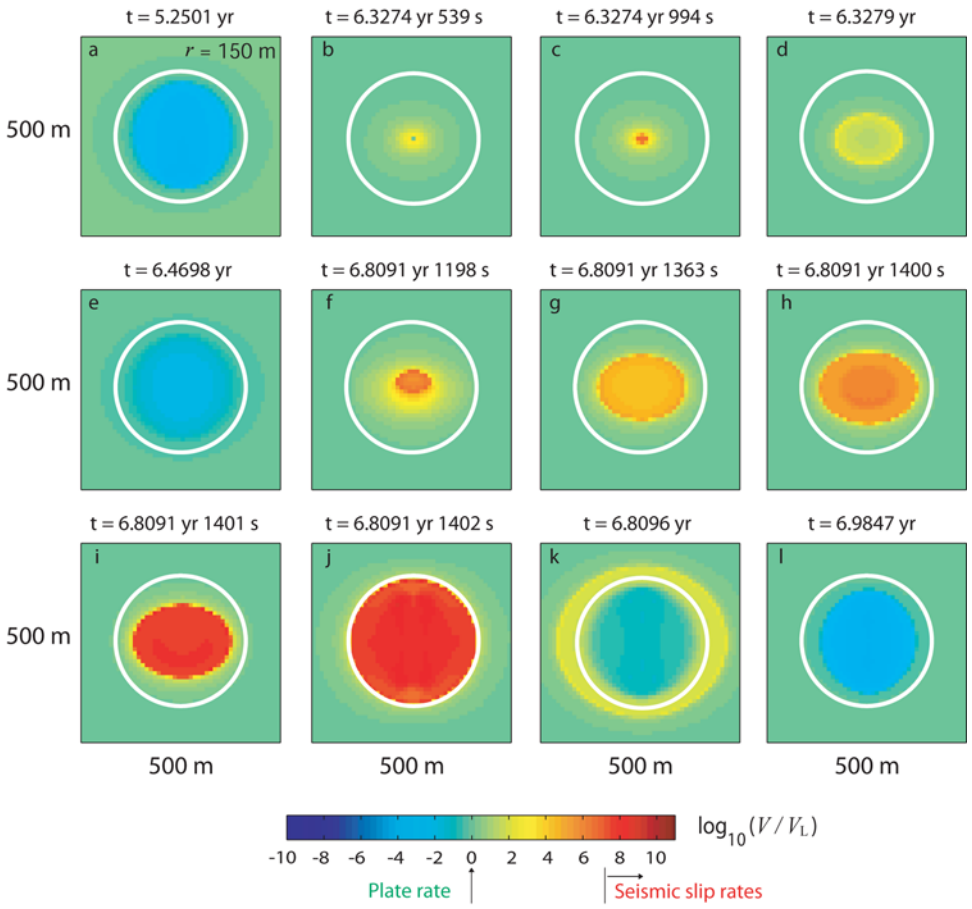

Figure 5. Snapshots of slip velocity distribution for one earthquake cycle and r = 150 m. Colors and markings have the same meanings as in Figure 3. The simulated fault region is 1200 m × 1200 m; only a part of it is shown in each snapshot. As in the case of r = 124 m (Figure 3), there is significant aseismic slip over the entire patch, and seismic slip eventually initiates from the middle of the patch. However, unlike in the case of r = 124 m, seismic slip extends over the entire patch.

the simulated time progresses, the locked area shrinks because of penetration of stable slip from the velocity-strengthening zone surrounding the patch (Figures 6a and 6b), as in the previous cases. However, slip acceleration starts close to the boundary of the patch (Figures 6c and 6d) and seismic slip initiates when a significant part of the patch is still locked (Figure 6e). The seismic event then propagates unidirectionally through the patch (Figures 6e–6h). This is different from the cases of smaller patches in Figures 3 and 5, where seismic slip initiates from the middle of the patch. Postseismic slip follows the dynamic event, both on and off the patch (Figures 6i–6k). In this case, the moment magnitude of seismic events is M_w = 3.7, the interseismic time is 2.17 years, and the ratio of seismic to total moment on the patch is about 0.8. The behavior of the velocity-weakening patch qualitatively resembles that of the fault model by Lapusta and Liu (submitted manuscript, 2008), where much larger fault dimensions and characteristic slips L are used to simulate large strike-slip earthquakes. Large values of L were used by Lapusta and Liu (submitted manuscript, 2008) for numerical tractability. Note that the half size of the actively slipping zone when seismic slip velocities are reached is about 130 m in the inplane (Mode II) direction and about 90 m in the antiplane (Mode III) direction (Figure 6e), with the latter value being very close to the critical patch radius of 83 m.

[14] The patterns of seismic and aseismic slip can exhibit additional complexity. The behavior shown in Figures 5b–5d corresponds to the increase of maximum slip velocity in Figure 2d between larger repeating earthquakes. Such increases in the interseismic period occur for some patch radii, as in our example with r = 150 m, but not others, and these transients are often completely aseismic. When they do develop slip velocities that we treat as seismic, their seismic moment is orders of magnitude smaller than that of the larger repeating events that occur in the same simulations. In such cases, we use the larger events to infer the seismic moment and recurrence interval. Note that even if we counted the occasional much smaller events as part of the repeating earthquake sequence and included them in the computation of the repeat time and average seismic moment for each repeating sequence, the resulting values would still be consistent, within the scatter, with the scaling discussed in the next section. Another type of complex response arises for patches that are large enough to retain a locked region before the dynamic event, such as our example with r = 350 m. After the aseismic slip penetrates into the patch, an aseismic transient propagates along the

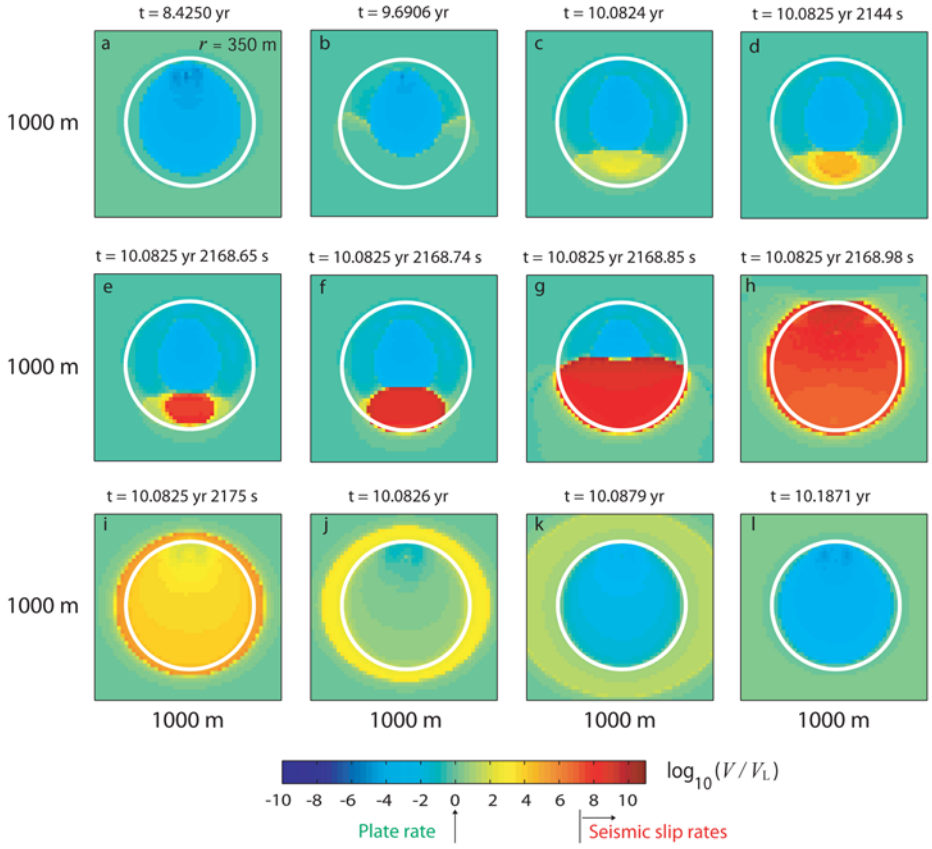

Figure 6. Snapshots of slip velocity distribution for one earthquake cycle and r = 350 m. Colors and markings have the same meanings as in Figures 3 and 5. The simulated fault region is 2000 m × 2000 m; only a part of it is shown in each snapshot. Aseismic slip on the patch before the event is restricted to the annulus close to the edges of the patch. The middle part of the patch is locked when the seismic event begins. The seismic slip initiates at one end of the patch and propagates unidirectionally.

creeping rim of the patch. Figure 6b actually shows such a transient in action, with its two fronts (appearing in light yellow color) propagating to the top on both sides of the locked patch. Such transients are discussed in more detail by Lapusta and Liu (submitted manuscript, 2008).

[15] Note that most (more than 90%) of the seismic slip (and seismic moment) in our simulations is confined to the velocity-weakening patch. For example, for r = 350 m, which is the largest patch size we have simulated, 95% of seismic slip occurs on the patch. This is because we assume a sharp transition between the velocity-weakening patch and the velocity-strengthening surroundings, as would be appropriate for an inclusion of a velocity-weakening material in an otherwise velocity-strengthening fault, and the dynamic rupture arrests right after exiting the velocity-weakening patch. Other scenarios could be envisioned, such as a gradual change in rate and state properties, which might lead to more seismic slip outside the patch.

4. Simulated Scaling of Seismic Moment With Recurrence Time

[16] To produce repeating earthquakes of different sizes, and hence to determine the scaling of seismic moment with the recurrence time in this model, we change the radius r of the velocity-weakening patch, keeping all other model parameters the same. The resulting scaling is plotted in Figure 7a, for r between 88 and 350 m. The lines corresponding to the observed scaling (equation (1)) and the theoretical scaling (equation (2)) are shown for comparison. For the long-term slip velocity V_L = 23 mm/a [*Nadeau and Johnson*, 1998], the model reproduces the right scaling exponent; the best fit (green line in Figure 7a) to the simulated results (blue dots in Figure 7a) gives $T \propto M_0^{0.19}$, very close to the observed $T \propto M_0^{0.17}$. However, this value of V_L results in smaller recurrence times than the observed ones. For V_L = 4.5 mm/a (Figure 7a, red dots), our model reproduces both the scaling and the absolute values of the observed recurrence times. The value V_L = 4.5 mm/a is within the range of 4 to 35 mm/a suggested for the portion of the San Andreas fault with repeating earthquakes [*Harris and Segall*, 1987].

[17] The main difference between our simulations and the theoretical model leading to scaling (2) is the significant aseismic slip that occurs in our model on the velocity-weakening patch, as discussed in section 3 for several examples. The ratio of seismic moment M_0 to the total moment M_{total} released on the patch during one earthquake cycle, as a function of the seismic moment M_0, is shown in Figure 8 for V_L = 23 mm/a. The ratio varies from 0.001 for the case with the smallest simulated events (r = 88 m) to 0.8

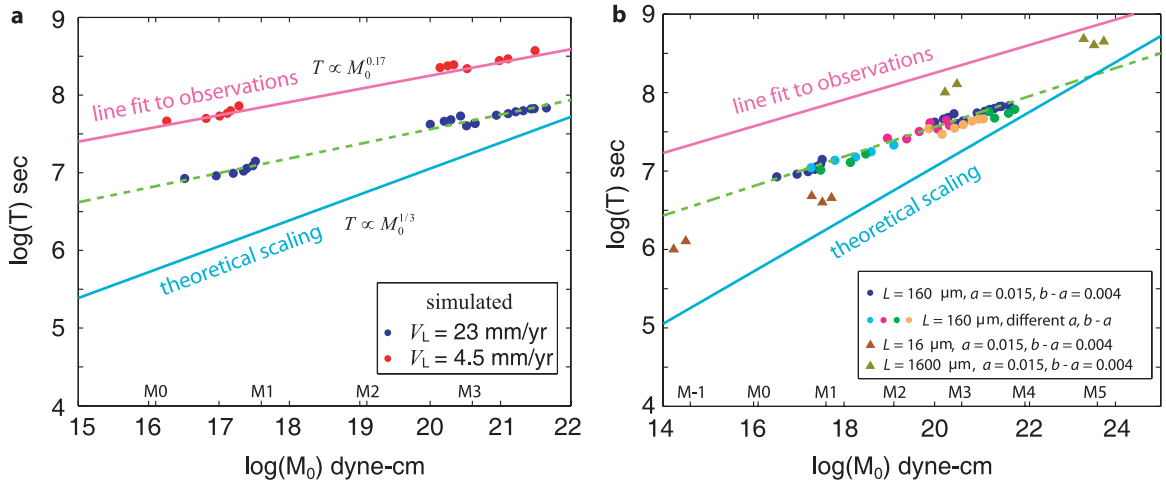

Figure 7. Scaling of seismic moment M_0 with recurrence time T for different patch radii r. (a) Simulation results for long-term slip velocities V_L of 23 mm/a and 4.5 mm/a are shown as blue and red dots, respectively. For each V_L, earthquakes of different sizes are obtained by varying the radius of the velocity-weakening patch; all other model parameters are the same. The lines fit to observations (equation (1)) of *Nadeau and Johnson* [1998] and the scaling (equation (2)) in the simple theoretical model are indicated by the magenta and light blue lines, respectively. The best fit to simulations with V_L = 23 mm/a is shown by the green dashed line. For both values of V_L, the observed scaling exponent is reproduced; the simulations with V_L = 4.5 mm/a also fit the absolute values of the recurrence times. (b) Simulation results for V_L = 23 mm/a, L = 160 μm, and several different combinations of rate and state parameters a and b all produce the same scaling, with events of all magnitudes between M_w = 0.3 and M_w = 3.7. V_L = 23 mm/a was used for computational efficiency. Simulations for different values of L also reproduce the observed scaling exponent.

for the case with the largest simulated events (r = 350 m). Hence, even for the largest events in Figures 7a and 8, a significant part, about 20%, of moment is released aseismically. Note that the results separate into two clusters (Figures 7a and 8). The cluster with smaller seismic moments corresponds to simulations in which repeating earthquakes occupy only a portion of the patch size, occurring close to its center, as described in section 3.1. The cluster with larger seismic moments corresponds to simulations in which the repeating earthquakes occupy the entire patch, as described in section 3.2.

[18] For a fixed set of friction properties, simulations with larger seismic moment, and hence with larger patches, generally correspond to larger proportions of seismic slip, with some scatter (Figure 8). However, when friction properties vary from patch to patch, the correspondence between larger patches and larger ratio of seismic to total slip, in general, no longer holds even approximately. This is because the ratio of seismic to total moment at least in part depends on the relative size of the patch with respect to the critical patch size, and the critical patch size would, in general, be different for different sets of friction parameters. Hence a given patch can result in different ratios of seismic to total moment, depending on its friction properties.

[19] The simulations reported so far have been done for a particular selection of rate and state parameters which are representative of laboratory results: L = 160 μm, a = 0.015 and $b - a$ = 0.004 for the velocity-weakening patch, and a = 0.019 and $a - b$ = 0.004 for the surrounding velocity-strengthening zone. To investigate how the behavior varies with friction parameters, we have explored a range of values for the rate and state parameters a and b, making the velocity-weakening parameter ($b - a$) on the patch two times larger and two times smaller and studying a different value of a. Sets of a and ($b - a$) on the velocity-weakening patch are: 0.015 and 0.004, 0.015 and 0.002, 0.015 and 0.008, 0.01 and 0.004, 0.01 and 0.002. In each case, the properties of the velocity-strengthening zone are assigned

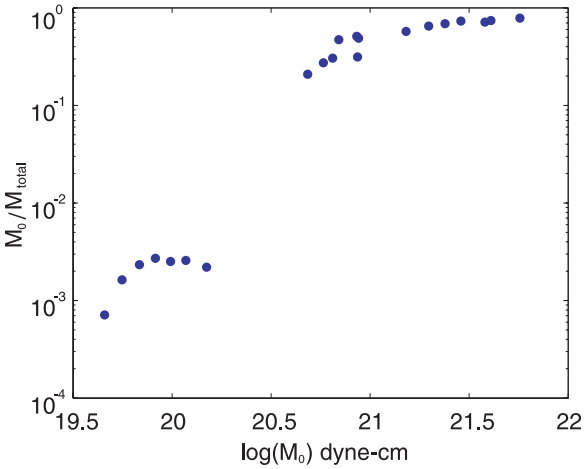

Figure 8. Ratio of seismic moment M_0 and total moment M_{total} released on the patch for one earthquake cycle as a function of the seismic moment M_0 for the simulations of Figure 7 with V_L = 23 mm/a. For all simulated cases, a significant portion of the total moment on the patch is released aseismically, from 0.999 to 0.2.

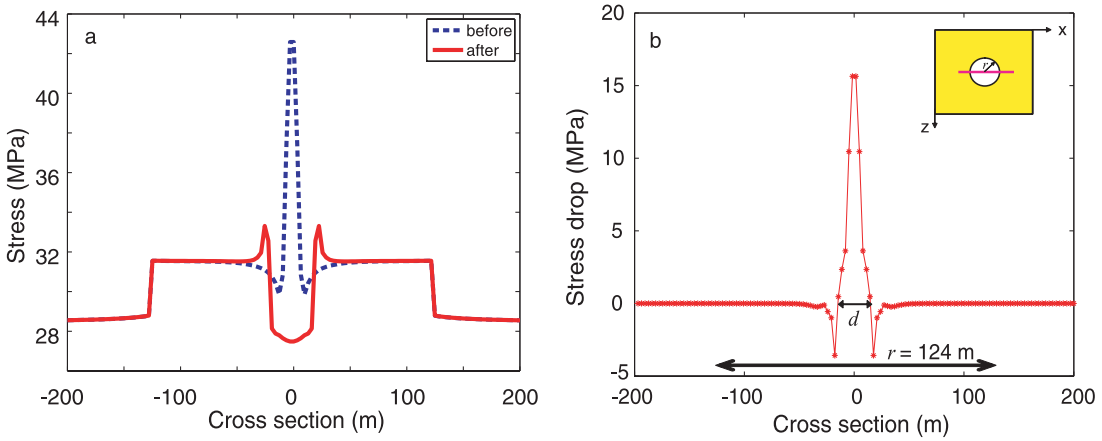

Figure 9. (a) Stress distribution along a cross section of the model, before (dashed line) and after (solid line) an event, for r = 124 m. (b) Static stress drop along the cross section. Inset shows the fault cross section indicated by a horizontal line through the center of the patch.

by switching the values of a and b. Remarkably, all of these simulations produce the same scaling of recurrence time with seismic moment, as shown in Figure 7b, resulting in events of all sizes between moment magnitudes from 0.3 to 3.7 for the patch sizes we simulated. (Larger events can be obtained using larger patches.) Note that the long-term slip velocity of 23 mm/a was used for this exploration, because computations with that velocity require less computational resources; simulations with 4.5 mm/a should produce exactly the same qualitative result but with longer recurrence times, matching the simulated results with observations as in Figure 7a.

[20] For different values of the characteristic slip L, our model continues to reproduce the scaling exponent but the absolute values of seismic moment and recurrence time change as indicated in Figure 7b. Note that a larger value of L results not only in larger recurrence times but also in larger velocity-weakening patches being able to slip aseismically, causing larger critical patch sizes and larger moments for the smallest earthquakes that can occur in the model. If L is increased from 160 μm to 1600 μm, a value outside the range of L observed in the laboratory, the smallest seismic event that arises in the model has the moment magnitude 2.8 which is larger than the smallest repeating earthquakes observed in Parkfield. Hence increasing L in the model is not a productive way of increasing recurrence times.

[21] The study of a range of rate and state parameters confirms the conclusion that the long-term slip velocity has to be smaller than 23 mm/a for the model, in its current form, to fit the absolute values of the recurrence times. However, it is possible that the model can be modified to match the recurrence times even for V_L = 23 mm/a as discussed in section 6.

5. Simulated Source Parameters

[22] The source dimensions of simulated repeating earthquakes of moment magnitudes 0.3 to 3.7 are in tens to hundreds of meters. We can find the (static) stress drop in the model by computing the difference in shear stresses before and after an event. For the simulation with r = 124 m (section 3.1, Figure 3), the shear stress distribution before and after a dynamic event, and the resulting static stress drop, over a cross section centered on the patch are shown in Figure 9. The stress drop is highly variable over the source region, with the negative stress drop, i.e., stress increase, outside the area of seismic slip. The heterogeneous stress drop distribution is qualitatively consistent with a recent seismic study for a M_w 2.1 repeating sequence in Parkfield [*Dreger et al.*, 2007]. For this and all other repeating earthquakes we simulated, the average stress drop over the area of positive stress drop is between 1 and 10 MPa (Figure 10). The values of stress drops and seismic source dimensions in our model are within the range of typical seismic estimates for small earthquakes [*Abercrombie*,

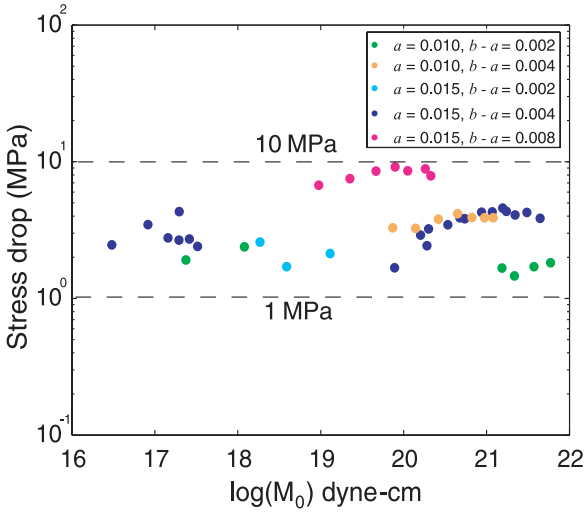

Figure 10. Stress drops averaged over the source (i.e., the area of positive stress drop) for all simulations with L = 160 μm. The stress drops are in the range 1–10 MPa of typical stress drops, consistently with recent inversions for small repeating earthquakes.

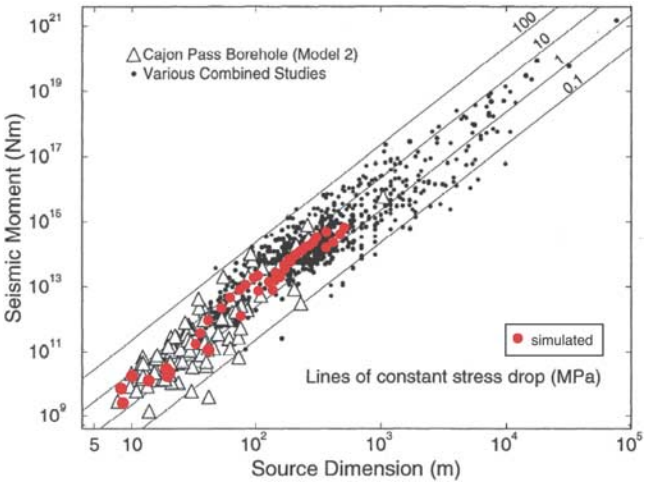

Figure 11. Values of seismic moment and source dimensions, calculated from our simulations with $L = 160$ μm and plotted on top of seismic estimates for small and medium earthquakes [*Abercrombie*, 1995]. The source parameters in our simulations are consistent with the seismic observations.

1995], as shown in Figure 11. The source parameters in our model are also consistent with inversions for the repeating earthquakes at Parkfield [*Imanishi et al.*, 2004; *Allmann and Shearer*, 2007].

6. Conclusions

[23] We find that representative rate and state friction parameters combined with a mechanically realistic earthquake model reproduce well-documented properties of small repeating earthquakes for reasonable values of the long-term slip velocity. The model incorporates all stages of slip development on faults and all inertial effects during seismic events. For the range of parameters studied, the simulations have produced repeating earthquakes with moment magnitudes from 0.3 to 3.7, and all of them follow the scaling (1) of the seismic moment with the recurrence time observed for small repeating earthquakes at Parkfield. At the same time, the simulated repeating earthquakes have source parameters that are similar to the ones inferred for repeating earthquakes at Parkfield and typical for small earthquakes in general. We find significant aseismic slip on the patch that also produces repeating earthquakes, ranging from more than 99% of total slip for the smallest repeating earthquakes that arise in our model (with moment magnitude 0.3) to 20% of total slip for the largest repeating earthquakes that we have simulated (moment magnitude 3.7). From stability properties of rate and state faults, it is clear that the smallest velocity-weakening patches capable of producing seismic slip would also have significant aseismic slip, since even smaller patches would be completely aseismic. That consideration, in fact, motivated the present study, which shows that significant aseismic slip persists over several earthquake magnitudes.

[24] The success of the model in matching the observed scaling of repeating earthquakes while producing reasonable source parameters is, in fact, due to the occurrence of significant aseismic slip at the location of seismic events. Hence any factors that can affect the proportion of aseismic and seismic slip in the model need to be explored, such as state variable evolution laws other than the aging formulation adopted in this study or additional weakening of frictional resistance during earthquakes due to shear heating. Note that the presence of the surrounding velocity-strengthening region is an important factor in inducing aseismic slip on the patch, since the slow slip from that region continuously penetrates into the patch because of stress concentrations at the boundary between slipping and locked areas. If that factor is a dominant one in inducing aseismic slip on the patch, then our model should produce qualitatively similar results with other rate and state formulations, especially if they retain properties of the "aging" law at near-plate slip velocities that govern the penetration of slow slip into the patch. Another important aspect to explore is the patch geometry. The streak-like nature of earthquake locations on creeping faults indicates that velocity-weakening fault materials may be present in stripes (W. Ellsworth, private communication, 2007). Hence a model that obtains earthquakes of different magnitudes by considering rectangular patches of a fixed width and increasing aspect ratio would be an interesting alternative to the increasing circular patches considered in this work.

[25] To match the absolute values of the observed recurrence times, our model requires a lower long-term slip rate, 4.5 mm/a, than the rate of 23 mm/a preferred in previous studies. The value $V_L = 4.5$ mm/a is within the range of 4 to 35 mm/a suggested for the portion of the San Andreas fault with repeating earthquakes [*Harris and Segall*, 1987]. Since repeating earthquakes occur in the transition region next to the partially locked segment that produces occasional Mw 6.0 Parkfield earthquakes, it is indeed possible that the local slip rate there is lower than the overall long-term rate of the creeping segment. Our model supports such lower slip rate. The discrepancy in the accumulated slip may be accounted for by penetration of seismic slip or afterslip. Another factor that would promote smaller creeping rates is additional shielding due to more local locked asperities that are larger than the observed repeating earthquakes, as proposed by *Sammis and Rice* [2001]. Hence it is important to understand how our model would combine with the ideas of *Sammis and Rice* [2001]. At the same time, it is possible that modifications in the considered friction law (a significantly different parameter regime, inclusion of inelastic dilatancy or strong dynamic weakening) might preserve the simulated scaling but lengthen the recurrence time, allowing our model to match the absolute values of the observed recurrence times with higher values of long-term slip rate closer to 23 mm/a.

[26] The study underscores the importance of properly accounting for interaction of seismic and aseismic slip in earthquake models. Recent observations suggest that similar interaction occurs on larger spatial scales, with aseismic slip transients and seismic tremor discovered on several seismogenic faults [*Kao et al.*, 2005; *Shelly et al.*, 2006; *Schwartz and Rokosky*, 2007]. Models conceptually similar to the one presented in this work but with more complex distributions of velocity-weakening and velocity-strengthening regions

may be able to explain a wide range of seismic and aseismic slip patterns observed.

[27] **Acknowledgments.** This study was supported by the U.S. Geological Survey (grant 07HQGR0070) and the National Science Foundation (grant EAR 0548277). The numerical simulations for this research were performed on the Caltech Division of Geological and Planetary Sciences Dell cluster. We thank Yi Liu for help with the code used to perform the simulations and Stephen Hickman for providing the SAFOD schematics for Figure 1. We also thank Bill Ellsworth, Allan Rubin, Paul Segall, Roland Bürgmann, Peter Shearer, Emily Brodsky, and an anonymous reviewer for comments and discussions that helped improve the paper.

References

Abercrombie, R. E. (1995), Earthquake source scaling relationships from −1 to 5 M_L using seismograms recorded at 2.5-km depth, *J. Geophys. Res.*, *100*, 24,015–24,036.

Allmann, B. P., and P. M. Shearer (2007), Spatial and temporal stress drop variations in small earthquakes near Parkfield, California, *J. Geophys. Res.*, *112*, B04305, doi:10.1029/2006JB004395.

Ampuero, J.-P., and A. M. Rubin (2008), Earthquake nucleation on rate and state faults-Aging and slip laws, *J. Geophys. Res.*, *113*, B01302, doi:10.1029/2007JB005082.

Anooshehpoor, A., and J. N. Brune (2001), Quasi-static slip-rate shielding by locked and creeping zones as an explanation for small repeating earthquakes at Parkfield, *Bull. Seismol. Soc. Am.*, *91*, 401–403.

Bayart, E., A. M. Rubin, and C. Marone (2006), Evolution of fault friction following large velocity jumps, *Eos Trans. AGU*, *87*(52), Fall Meet. Suppl., Abstract S31A-0180.

Beeler, N. M., T. E. Tullis, and J. D. Weeks (1994), The roles of time and displacement in the evolution effect in rock friction, *Geophys. Res. Lett.*, *21*, 1987–1990.

Beeler, N. M., D. L. Lockner, and S. H. Hickman (2001), A simple stick-slip and creep-slip model for repeating earthquakes and its implication for microearthquakes at Parkfield, *Bull. Seismol. Soc. Am.*, *91*, 1797–1804.

Bürgmann, R., D. Schmidt, R. M. Nadeau, M. d'Alessio, E. Fielding, D. Manaker, T. V. McEvilly, and M. H. Murray (2000), Earthquake potential along the northern Hayward fault, California, *Science*, *289*, 1178–1182.

Chen, K. H., R. M. Nadeau, and R.-J. Rau (2007), Towards a universal rule on the recurrence interval scaling of repeating earthquakes?, *Geophys. Res. Lett.*, *34*, L16308, doi:10.1029/2007GL030554.

Day, S. M., L. A. Dalguer, N. Lapusta, and Y. Liu (2005), Comparison of finite difference and boundary integral solutions to three-dimensional spontaneous rupture, *J. Geophys. Res.*, *110*, B12307, doi:10.1029/2005JB003813.

Dieterich, J. H. (1979), Modeling of rock friction: 1. Experimental results and constitutive equations, *J. Geophys. Res.*, *84*, 2161–2168.

Dieterich, J. H. (1981), Constitutive properties of faults with simulated gouge, in *Mechanical Behavior of Crustal Rocks*, *Geophys. Monogr. Ser.*, vol. 24, edited by N. L. Carter et al., pp. 103–120, AGU, Washington, D. C.

Dieterich, J. H. (1992), Earthquake nucleation on faults with rate-dependent and state-dependent strength, *Tectonophysics*, *211*, 115–134.

Dieterich, J. H. (2007), Applications of rate-and-state-dependent friction to models of fault slip and earthquake occurrence, in *Treatise on Geophysics*, vol. 4, edited by H. Kanamori, pp. 107–129, Elsevier, Amsterdam.

Dreger, D., R. M. Nadeau, and A. Chung (2007), Repeating earthquake finite source models: Strong asperities revealed on the San Andreas fault, *Geophys. Res. Lett.*, *34*, L23302, doi:10.1029/2007GL031353.

Ellsworth, W. L., and L. D. Dietz (1990), Repeating earthquakes: Characteristics and implications, in *Proceedings of Workshop XLVI: The 7th U.S.-Japan Seminar on Earthquake Prediction*, *U.S. Geol. Surv. Open File Rep.*, *90–98*, 226–245.

Harris, R. A., and P. Segall (1987), Detection of a locked zone at depth on the Parkfield, California, segment of the San Andreas fault, *J. Geophys. Res.*, *92*, 7945–7962.

Hickman, S., M. Zoback, and W. Ellsworth (2004), Introduction to special section: Preparing for the San Andreas Fault Observatory at depth, *Geophys. Res. Lett.*, *31*, L12S01, doi:10.1029/2004GL020688.

Igarashi, T., T. Matsuzawa, and A. Hasegawa (2003), Repeating earthquakes and interplate aseismic slip in the northeastern Japan subduction zone, *J. Geophys. Res.*, *108*(B5), 2249, doi:10.1029/2002JB001920.

Imanishi, K., W. L. Ellsworth, and S. G. Prejean (2004), Earthquake source parameters determined by the SAFOD pilot hole seismic array, *Geophys. Res. Lett.*, *31*, L12S09, doi:10.1029/2004GL019420.

Kao, H., S. J. Shan, H. Dragert, G. Rogers, J. F. Cassidy, and K. Ramachandran (2005), A wide depth distribution of seismic tremors along the northern Cascadia margin, *Nature*, *436*, 841–844.

Kato, N. (2004), Interaction of slip on asperities: Numerical simulation of seismic cycles on a two-dimensional planar fault with nonuniform frictional property, *J. Geophys. Res.*, *109*, B12306, doi:10.1029/2004JB003001.

Kato, N., and T. E. Tullis (2001), A composite rate- and state-dependent law for rock friction, *Geophys. Res. Lett.*, *28*, 1103–1106.

Lapusta, N., J. R. Rice, Y. Ben-Zion, and G. T. Zheng (2000), Elastodynamic analysis for slow tectonic loading with spontaneous rupture episodes on faults with rate- and state-dependent friction, *J. Geophys. Res.*, *105*, 23,765–23,789.

Marone, C. (1998), Laboratory-derived friction laws and their application to seismic faulting, *Ann. Rev. Earth Planet. Sci.*, *26*, 643–696.

Marone, C., J. E. Vidale, and W. L. Ellsworth (1995), Fault healing inferred from time-dependent variations in source properties of repeating earthquakes, *Geophys. Res. Lett.*, *22*, 3095–3098.

Matsubara, M., Y. Yagi, and K. Obara (2005), Plate boundary slip associated with the 2003 off-Tokachi earthquake based on small repeating earthquake data, *Geophys. Res. Lett.*, *32*, L08316, doi:10.1029/2004GL022310.

Nadeau, R. M., and L. R. Johnson (1998), Seismological studies at Parkfield VI: Moment release rates and estimates of source parameters for small repeating earthquakes, *Bull. Seismol. Soc. Am.*, *88*, 790–814.

Nadeau, R. M., and T. V. McEvilly (1999), Fault slip rates at depth from recurrence intervals of repeating microearthquakes, *Science*, *285*, 718–721.

Nadeau, R. M., A. Michelini, R. A. Uhrhammer, D. Dolenc, and T. V. McEvilly (2004), Detailed kinematics, structure and recurrence of micro-seismicity in the SAFOD target region, *Geophys. Res. Lett.*, *31*, L12S08, doi:10.1029/2003GL019409.

Peng, Z., and Y. Ben-Zion (2005), Spatiotemporal variations of crustal anisotropy from similar events in aftershocks of the 1999 *M*7.4 İzmit and *M*7.1 Düzce, Turkey, earthquake sequences, *Geophys. J. Int.*, *160*, 1027–1043.

Rice, J. R., and A. L. Ruina (1983), Stability of steady frictional slipping, *J. Appl. Mech.*, *50*, 343–349.

Rubin, A. M., and J.-P. Ampuero (2005), Earthquake nucleation on (aging) rate and state faults, *J. Geophys. Res.*, *110*, B11312, doi:10.1029/2005JB003686.

Ruina, A. (1983), Slip instability and state variable friction laws, *J. Geophys. Res.*, *88*, 359–370.

Sammis, C. G., and J. R. Rice (2001), Repeating earthquakes as low-stress-drop events at a border between locked and creeping fault patches, *Bull. Seismol. Soc. Am.*, *91*, 532–537.

Schaff, D. P., and G. C. Beroza (2004), Coseismic and postseismic velocity changes measured by repeating earthquakes, *J. Geophys. Res.*, *109*, B10302, doi:10.1029/2004JB003011.

Schaff, D. P., G. C. Beroza, and B. E. Shaw (1998), Postseismic response of repeating aftershocks, *Geophys. Res. Lett.*, *25*, 4549–4552.

Schwartz, S. Y., and J. M. Rokosky (2007), Slow slip events and seismic tremor at circum-Pacific subduction zones, *Rev. Geophys.*, *45*, RG3004, doi:10.1029/2006RG000208.

Shelly, D. R., G. C. Beroza, S. Ide, and S. Nakamula (2006), Low-frequency earthquakes in Shikoku, Japan, and their relationship to episodic tremor and slip, *Nature*, *442*, 188–191.

Vidale, J. E., W. L. Ellsworth, A. Cole, and C. Marone (1994), Variations in rupture process with recurrence interval in a repeated small earthquake, *Nature*, *368*, 624–626.

T. Chen, Seismological Laboratory, California Institute of Technology, Pasadena, CA 91125, USA. (tchen@caltech.edu)

N. Lapusta, Division of Engineering and Applied Science and Seismological Laboratory, California Institute of Technology, Pasadena, CA 91125, USA. (lapusta@its.caltech.edu)